

Hardware Implementation of a Predictive DTC-SVM with a Sliding Mode Observer of an Induction Motor on the FPGA

* Saber KRIM, ** Soufien GDAIM, *** Abdellatif MTIBAA and **** Mohamed Faouzi MIMOUNI
*,**,*** Laboratory of Electronics and Microelectronics, Faculty of Sciences, University of Monastir,
Tunisia

**** Research Unit "Industrial systems Study and renewable energy". University of Monastir, Tunisia
**** The National Engineering School of Monastir Ibn El jazaar City, 5019, Monastir, Tunisia

Abstract: - The first objective of this research is to present an improved Direct Torque Control based on the Space Vector Modulation (DTC-SVM) and a Sliding Mode Observer (SMO). The disadvantages of the conventional Direct Torque Control (DTC) are the high ripples for the electromagnetic torque and the stator flux, as well as the distortions of the stator current. To solve these problems, we have used the approach of the (DTC) based on the space vector modulation. Also, one of the major problems for controlling induction machines is the lack of knowledge about the real values of some parameters, such as the stator resistance which is subjected to large variations during the operation. To follow the change in the internal state of the system and the stator resistance we use a technique based on the SMO. This technique overcomes the limitations of the open-loop estimator, like the adaptation of the variation of the stator resistance at a low speed, the correction of measurement errors of the stator currents, and the estimation errors of the stator flux. The second objective is to propose a novel method for implementing a DTC-SVM with an SMO on the Field Programmable Gate Array (FPGA). The advantages of this method are not only the simulation, control and testing of the correct operation, but also the development of a discrete algorithm and the generation of the Very-high-speed integrated circuits Hardware Description Language (VHDL) code which can be implemented on the FPGA. The performances of the DTC-SVM with an SMO are evaluated by digital simulation and developed to be implemented on Xilinx Virtex-V FPGA with an xc5vfx70t-3ff1136 package using the toolbox Xilinx system generator.

Key-Words: - Direct Torque Control (DTC), predictive controller, Space Vector Modulation (SVM), induction motor, Sliding Mode Observer (SMO), Xilinx System Generator (XSG), Field Programmable Gate Array (FPGA).

1 Introduction

Nowadays, the competition on the market requires new industrial systems with higher performances. At the same time the cost must be acceptable. To reduce the cost, the time-to-market, the price of the controller device and its energy consumption must be reduced. It is too difficult to decrease the cost, given that the new industrial control system needs computing resources and reduced execution time. To solve this problem, two main families of control devices are used: the software solutions, like the Digital Signal Processor (DSP) controllers, and the microcontrollers and hardware solutions, like the Field Programmable Gate Array (FPGA). The microcontrollers and DSP controllers integrate a microprocessor core and several peripherals to communicate with the exterior environment. [1] and [2] present the difference between the

microcontrollers and the DSP controllers. The main limitation of these solutions is the difficulty to take advantage of the parallel processing. To overcome this limitation, an alternative family of available digital devices for the digital control of industrial systems is the FPGA [3]. An FPGA consists in an array of logic blocks interconnected by a general interconnection network. The main advantage of the FPGA, relative to the software solutions, is parallel processing. So due to its massive computation capability, the FPGA is the most used component to overcome the real-time constraints, mostly for the complex algorithms.

Induction machines are currently the most used machines in the industrial field thanks to their low cost, robustness, good performance and simple control [4]. They are used in multiple applications that require speed variation. The conventional Direct

Torque Control (DTC) is a new control technique developed and presented by [5], [6] and [7]. It is based on the orientation of the stator flux by a direct action on the states of the switches of the inverter [8], [9]. This technique is characterized by very fast dynamics [10]. On the one hand, the conventional DTC has some advantages:

- It does not require calculations in the reference (d, q)
- There is no calculation block voltage modulation (pulse width modulation).
- It is not necessary to make a current decoupling relative to voltages, as in the case of the Field Oriented Control (FOC)

On the other hand, it has some disadvantages as:

- The existence of the electromagnetic torque ripples
- The existence of the stator flux ripples
- The existence of a high distortion of the current
- The variation of the switching frequency.

To improve the performance of the conventional DTC in terms of ripples and variation in the switching frequency, the Direct Torque Control based on the Space Vector Modulation (DTC-SVM) technique was suggested in [11], [12]. The DTC-SVM utilizes a pure open loop integration having well-known problems of integration effects on digital systems, especially at a low speed operation range [13], [14], and it is sensitive to the variation of the stator resistance [15]. Therefore, many observation methods, like the high gain observer, the backstepping observer, the model reference-adaptive system and the extended kalman filter [16], are used to overcome these limitations. In this work, we propose to use the adaptive sliding mode observer (SMO) for the observation of the stator flux and the adaptation of the variation of the stator resistance. The observer has been introduced to replace the open-loop estimator of the stator flux. Furthermore, it has been provided with an adaptation mechanism of the stator resistance. Thus, the first objective of this research is, to give a fair comparison between the two techniques (conventional DTC and DTC-SVM) in terms of ripples of the stator flux and torque and in terms of high distortion at the waveform of the stator current. The second objective is, to give a fair comparison between a DTC-SVM with an open loop estimator and a DTC-SVM with a sliding mode observer at the adjustment stage of the stator resistance. Finally, the third objective is to implement the proposed model on the Xilinx Virtex-V FPGA, to enjoy the performances of the FPGAs in the field of digital

control of electrical machines in real time. The performance of the suggested model is proved by simulation and implementation results.

The organization of this paper is given as follows: In Section II, an overview of the hardware implementation method is presented. In Section III, the induction motor model and the conventional DTC principle are presented. In Section IV, the space vector modulation and the SMO are described. In Section V, the design of the SMO in XSG is presented. In Section VI, the simulation results of the predictive DTC-SVM with SMO using the XSG are presented and discussed. In Section VII the implementation results using the FPGA Virtex 5 are presented and discussed. Section VIII concludes this paper by discussing the overall results of the proposed control technique.

2 Description of the hardware implementation method

The objective of this study is to implement an algorithm of predictive DTC-SVM based on the Sliding Mode Observer (SMO) using the XSG blocks. It is a toolbox developed by Xilinx to be integrated into the Matlab-Simulink and it lets the user create parallel systems for the FPGA [17]. The created models are displayed in blocks and can be connected to other Matlab-Simulink blocks. Once the system is completed, the VHDL code generated by the XSG tool exactly reproduces the behavior observed in Matlab. The realized system must be simulated and verified quickly and often throughout the system development. So it is much easier to analyze the results with Matlab than with tools associated with Very-high-speed integrated circuits Hardware Description Language (VHDL), such as Modelsim. The XSG tool is used to produce a model that will immediately run on the hardware once completed and validated [18]. Fig.1 shows the broad flow design of the XSG. As already mentioned, you can then move to the configuration file to program the FPGA [19].

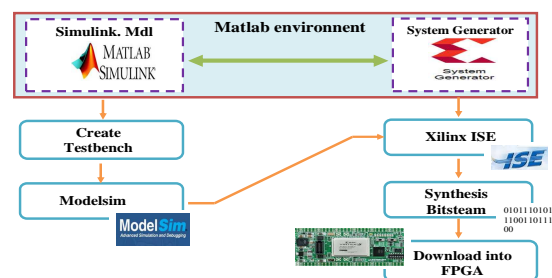


Fig. 1. XSG design flow

3 Conventional DTC of an induction motor

3.1 Induction machine model

The dynamic model of the induction machine can be represented in the (α, β) frame as:

$$\begin{cases} \frac{di_{s\alpha}}{dt} = \frac{R_s + R_r}{L_s L_r} i_{s\alpha} - \omega i_{s\beta} + \frac{R_r}{\sigma L_s L_r} \phi_{s\alpha} + \frac{\omega}{\sigma L_s} \phi_{s\beta} + \frac{1}{\sigma L_s} v_{s\alpha} \\ \frac{di_{s\beta}}{dt} = -\omega i_{s\alpha} + \frac{R_s + R_r}{L_s L_r} i_{s\beta} - \frac{\omega}{\sigma L_s} \phi_{s\alpha} + \frac{R_r}{\sigma L_s L_r} \phi_{s\beta} + \frac{1}{\sigma L_s} v_{s\beta} \\ \frac{d\phi_{s\alpha}}{dt} = -R_s i_{s\alpha} + v_{s\alpha} \\ \frac{d\phi_{s\beta}}{dt} = R_s i_{s\beta} + v_{s\beta} \end{cases} \quad (1)$$

with: $\sigma = 1 - \frac{L_m^2}{L_s L_r}$

The state model of an induction machine is given below:

$$\dot{X} = [A]X + [B]U \quad (2)$$

The state vector X is composed by a stator current and flux components. The vector command U is constituted by the stator voltage components. X and U are given as in the form of

$$X = [i_{s\alpha} \ i_{s\beta} \ \phi_{s\alpha} \ \phi_{s\beta}]^T, \quad v_s = [v_{s\alpha} \ v_{s\beta}]^T$$

3.2 Conventional DTC principle

The structure of the conventional DTC of the induction motor was introduced in 1986 by Takahashi.I. Depending on the position of the flux vector in one of the six sectors of the plane (α, β) , a truth table is used to define the optimum stator voltage vector to be applied to the motor. The components of the stator voltage vector $V_s (V_{s\alpha}, V_{s\beta})$ are based on three control variables (S_a, S_b, S_c) of the switches of the inverter and the DC supply voltage E by applying the transformation Concordia:

$$\begin{cases} V_{s\alpha} = \sqrt{\frac{2}{3}}U(S_a - \frac{1}{2}(S_b + S_c)) \\ V_{s\beta} = \sqrt{\frac{2}{3}}U(S_b - S_c) \end{cases} \quad (3)$$

$$\bar{v}_s = v_{s\alpha} + jv_{s\beta} \quad (4)$$

The magnitude of the stator flux is determined by calculating its components in the stationary reference, as shown by Eqs.(5) and (6):

$$\begin{cases} \phi_{s\alpha} = \int_0^t (v_{s\alpha} - R_s i_{s\alpha}) dt \\ \phi_{s\beta} = \int_0^t (v_{s\beta} - R_s i_{s\beta}) dt \end{cases} \quad (5)$$

$$\begin{cases} \phi_s = \sqrt{\phi_{s\alpha}^2 + \phi_{s\beta}^2} \\ \arg \phi_s = \arctg \frac{\phi_{s\beta}}{\phi_{s\alpha}} \end{cases} \quad (6)$$

The electromagnetic torque can be estimated from the components of the stator flux and the current in the fixed coordinate system (α, β) .

$$C_e = \frac{3}{2} p (\phi_{s\alpha} i_{s\beta} - \phi_{s\beta} i_{s\alpha}) \quad (7)$$

The choice of the control sequence applied to the switches of a three-phase voltage inverter is based essentially on the use of hysteresis comparators. The hysteresis bands allow avoiding unnecessary switching when the calculated error is very small. Thus, the stator flux vector is kept in a circular crown. The control sequence of the inverter switch voltage were then defined by [20], where the outputs of the hysteresis comparators E_ϕ and E_C and the sector number N_i presented the inputs of the switching table.

Table 1. Switching Table

E_ϕ	E_c	N1	N2	N3	N4	N5	N6
1	1	V2	V3	V4	V5	V6	V1
	0	V7	V0	V7	V0	V7	V0
	-1	V6	V1	V2	V3	V4	V5
0	1	V3	V4	V5	V6	V1	V2
	0	V0	V7	V0	V7	V0	V7
	-1	V5	V6	V1	V2	V3	V4

The structure of the conventional DTC of an induction motor is given, as shown by Fig. 2:

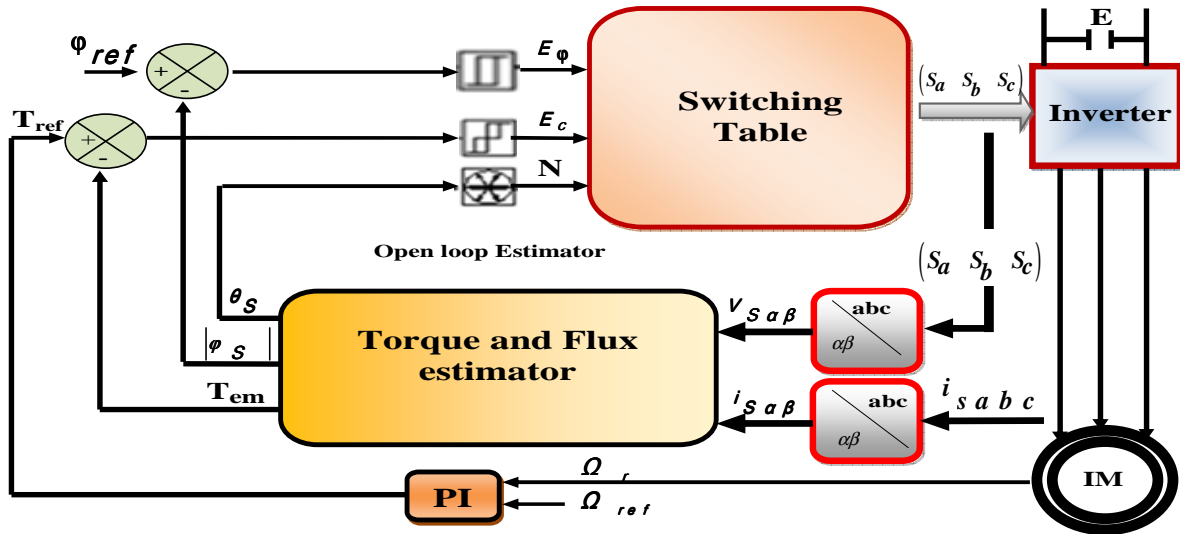


Fig. 2. Schematic of the conventional DTC

4 Predictive DTC-SVM of an induction motor

This control technique differs from the conventional DTC by using a Space Vector Modulation also which ensures operation at a constant modulation frequency to the converter. In this case, the torque is

controlled by a predictive controller where the switching table and the hysteresis comparators are eliminated. This method, we called a DTC with a constant frequency, reduces of torque and flux oscillations. The structure of the predictive DTC-SVM of an induction motor is given in Fig. 3.

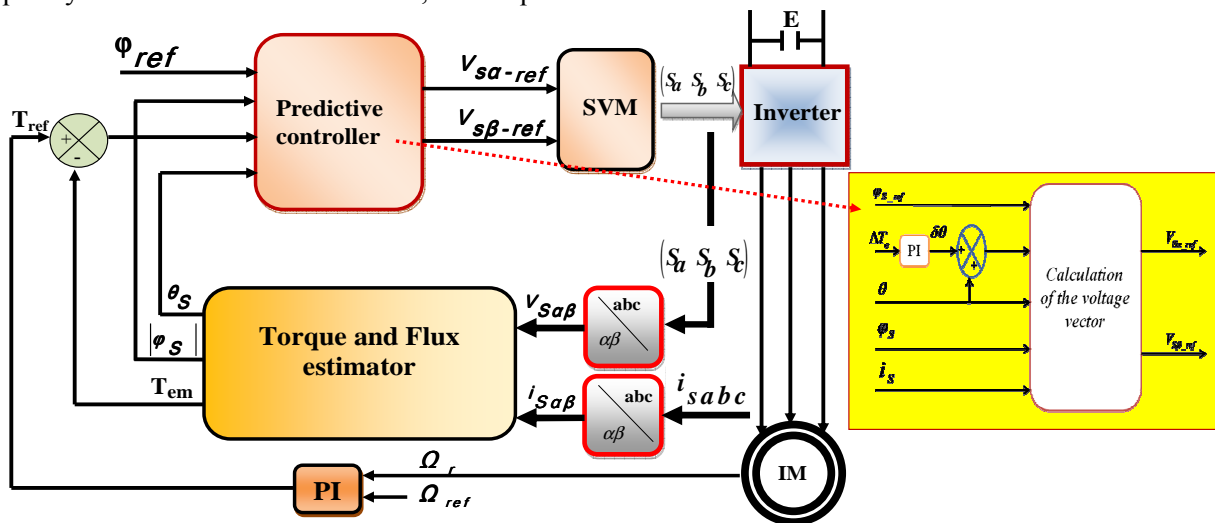


Fig. 3. Schematic of the predictive DTC-SVM

The relationship between the electromagnetic torque pulsation ΔT_{em} and the deviation of the stator flux φ_s from its reference φ_{sref} is given by Eq.(8) [21]:

$$\frac{\Delta T_e}{T_{eref}} = K_\varphi \frac{|\Delta \varphi_s|}{|\varphi_{sref}|} + K_\theta \Delta \theta \quad (8)$$

$$\Delta \varphi_s = |\varphi_{sref}| - |\varphi_s| \quad (9)$$

$$\Delta \theta = \angle \varphi_{sref} - \angle \varphi_s \quad (10)$$

where K_φ and K_θ are the constants derived from the induction motor specifications. T_{eref} is the reference of the electromagnetic torque.

The electromagnetic torque ripples are actually caused by $\Delta \varphi_s$ and $\Delta \theta_s$, but the influences of the $\Delta \varphi_s$ is smaller than that of the $\Delta \theta_s$. As a consequence the electromagnetic torque ripples can be almost removed if $\Delta \theta$ is kept close to zero.

We can notice in Eq.(8) that the relation between error of the electromagnetic torque and increment

angle $\Delta\theta$ is linear. Therefore a predictive controller is used to generate the load angle changes in order to reduce the error between the reference and the real electromagnetic torque. The diagram of the predictive controller is shown in Fig.3. The evolution of the stator flux vectors is given in Fig. 4.

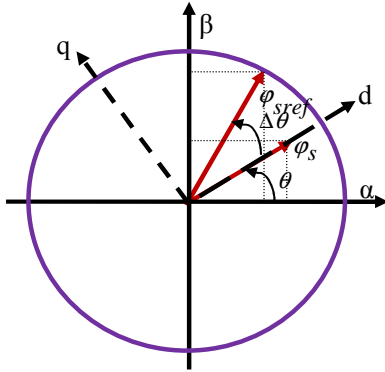


Fig. 4. Stator flux vectors φ_s and φ_{sref}

From the (α, β) axis, the components of the reference stator voltage are calculated as:

$$V_{S\alpha ref} = \frac{\varphi_{sref} \cos(\theta + \Delta\theta) - \varphi_s \cos(\theta)}{T_s} + R_s i_{S\alpha} \quad (11)$$

$$V_{S\beta ref} = \frac{\varphi_{sref} \sin(\theta + \Delta\theta) - \varphi_s \sin(\theta)}{T_s} + R_s i_{S\beta} \quad (12)$$

$$V_{sref} = \sqrt{V_{s\alpha ref}^2 + V_{s\beta ref}^2} \quad (13)$$

$$\theta = \arctg\left(\frac{\varphi_{s\beta}}{\varphi_{s\alpha}}\right) \quad (14)$$

4.1 SVM principle

For each modulation period of the inverter, the three-phase voltages provided by the control algorithm can be expressed in a stationary reference frame linked to the stator by using their projections $V_{S\alpha}$ and $V_{S\beta}$. A three-phase inverter with two voltage levels has six switching cells, giving eight possible switching configurations ($V_0, V_1, V_2, V_3, V_4, V_5, V_6$ and V_7). These latter configurations can be expressed in (α, β) by eight voltage vectors. In Fig. 5, it can be seen that the six active voltage vectors form the axes of a hexagon and two the zero voltage vectors are at the origin (center).

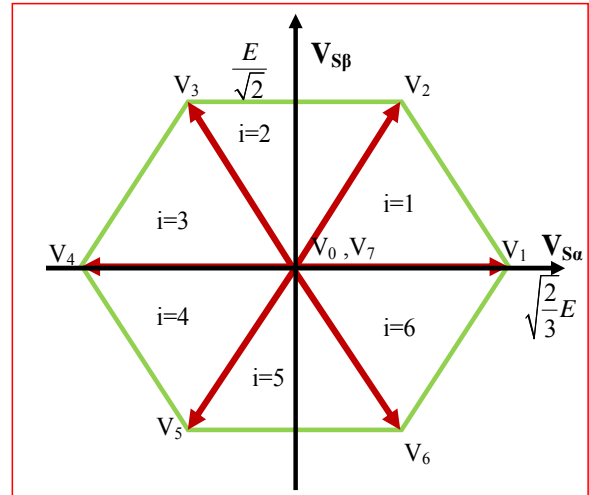


Fig. 5. Representation of voltage vectors in the coordinate (α, β)

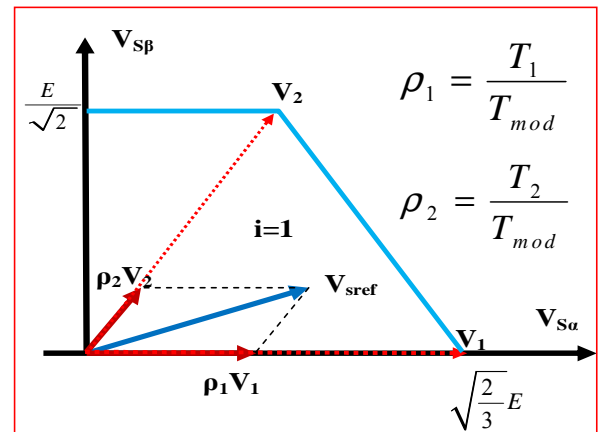


Fig. 6. Projection of a reference voltage vector sector 1 ($i=1$)

The sector is determined using the components of the voltage vector $(V_{s\alpha}, V_{s\beta})$ by the following equation:

$$\theta_s = \arctg\left(\frac{V_{s\beta}}{V_{s\alpha}}\right) \quad (15)$$

The SVM is shown in Fig. 6, where the desired voltage vector V_{sref} is projected on the two adjacent voltage vectors V_i and V_{i+1} . The values of these projections provide the determination of the desired commutation times T_i and T_{i+1} and correspond to two nonzero switching states of the inverter. The reference voltage vector in sector 1 can be expressed in the reference (α, β) by the following expression:

$$\vec{V}_{Sref} = V_{S\alpha} + jV_{S\beta} = \frac{T_1}{T_{mod}} \vec{V}_1 + \frac{T_2}{T_{mod}} \vec{V}_2 \quad (16)$$

$$\text{where } T_{mod} = T_1 + T_2 + T_0 \quad (17)$$

In sector 1, the expression of the voltage in the stator reference is:

$$\begin{aligned} \vec{V}_{Sref} = V_{S\alpha} + jV_{S\beta} = & \frac{T_1}{T_{mod}} \frac{\sqrt{2}}{\sqrt{3}} E(\cos(0)) \\ & + j\sin(0) + \frac{T_2}{T_{mod}} \frac{\sqrt{2}}{\sqrt{3}} (\cos(\frac{\pi}{3}) + j\sin(\frac{\pi}{3})) \end{aligned} \quad (18)$$

Using Eq.(15) the expressions of the times T_1 and T_2 are given below:

$$T_1 = (\sqrt{\frac{3}{2}} V_{S\alpha} - \frac{1}{\sqrt{2}} V_{S\beta}) \frac{T_{mod}}{E} \quad (19)$$

$$T_2 = \sqrt{2} V_{S\beta} \frac{T_{mod}}{E} \quad (20)$$

The calculation of the switching will be determined from the following cyclic reports:

$$\rho_i = \frac{T_i}{T_{mod}} \quad (21)$$

For sector 1, the cyclic reports ρ_1 and ρ_2 can be represented as

$$\rho_1 = \sqrt{\frac{3}{2}} \frac{V_{S\alpha}}{E} - \frac{1}{\sqrt{2}} \frac{V_{S\beta}}{E} \quad (22)$$

$$\rho_2 = \sqrt{2} \frac{V_{S\beta}}{E} \quad (23)$$

Fig. 7 shows the Space Vector pulse width modulation switching patterns in sector N_1 . The time duration of each nonzero vector is divided equally into two parts. The time duration of the zero vectors is distributed equally from V_0 to V_7 , and thus the switching sequence of the space vector is $V_0, V_1, V_2, V_7, V_7, V_2, V_1,$ and V_0 during the modulation period. This sequence can ensure that there is only one phase switch when the switching pattern switches, hence the ability to reduce the loss of switching devices and the harmonic component of the output current of the 3-phase inverter.

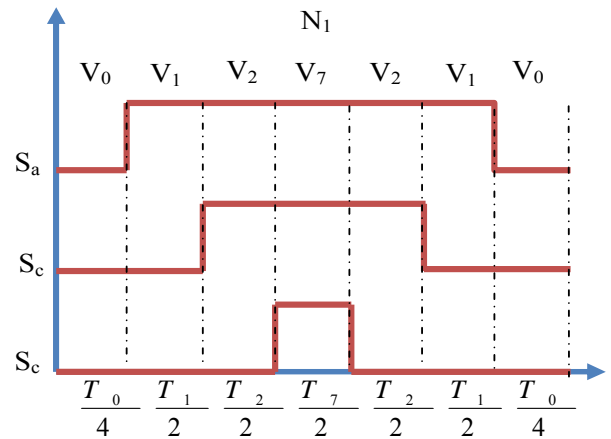


Fig. 7. Sequences of the switch states in sector N_1

For each phase of the inverter, the control sequences are given as follows:

$$\begin{cases} \rho_a = \rho_1 + \rho_2 + \frac{1}{2} \rho_0 \\ \rho_b = \rho_2 + \frac{1}{2} \rho_0 \\ \rho_c = \frac{1}{2} \rho_0 \end{cases} \quad (24)$$

As $\rho_1 + \rho_2 + \rho_0 = 1$

Using the Eqs.(22) and (23). Eq.(24) can be rewritten as

$$\begin{cases} \rho_a = \frac{1}{2} (1 + \sqrt{\frac{3}{2}} \frac{V_{S\alpha}}{E_0} + \frac{1}{\sqrt{2}} \frac{V_{S\beta}}{E_0}) \\ \rho_b = \frac{1}{2} (1 - \sqrt{\frac{3}{2}} \frac{V_{S\alpha}}{E_0} + \frac{1}{\sqrt{2}} \frac{V_{S\beta}}{E_0}) \\ \rho_c = \frac{1}{2} (1 - \sqrt{\frac{3}{2}} \frac{V_{S\alpha}}{E_0} - \frac{1}{\sqrt{2}} \frac{V_{S\beta}}{E_0}) \end{cases} \quad (25)$$

4.2 Predictive DTC-SVM of an induction motor with an SMO

The objective of the SMO is to construct the components of the stator flux vector and to provide the adaptation of the stator resistance. The principle of the SMO is given in Fig. 8.

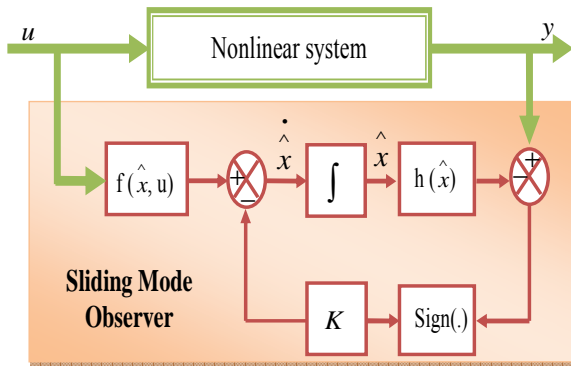


Fig. 8. SMO principle

The observation model of the induction motor can be represented in the (α, β) frame as follows:

$$\left\{ \begin{aligned} \frac{d \hat{i}_{s\alpha}}{dt} &= \frac{R_s + R_r}{L_s L_r} i_{s\alpha} - \omega i_{s\beta} + \frac{R_r}{\sigma L_r L_s} \hat{\varphi}_{s\alpha} \\ &+ \frac{\omega}{\sigma L_s} \hat{\varphi}_{s\beta} + \frac{1}{\sigma^* L_s} V_{s\alpha} + A_{11} I_{s1} + A_{12} I_{s2} \\ \frac{d \hat{i}_{s\beta}}{dt} &= \omega i_{s\alpha} + \frac{R_s + R_r}{L_s L_r} i_{s\beta} - \frac{\omega}{\sigma L_s} \hat{\varphi}_{s\alpha} \\ &+ \frac{R_r}{\sigma L_r L_s} \hat{\varphi}_{s\beta} + \frac{1}{\sigma^* L_s} V_{s\beta} + A_{21} I_{s1} + A_{22} I_{s2} \\ \frac{d \hat{\varphi}_{s\alpha}}{dt} &= -R_s i_{s\alpha} + v_{s\alpha} + A_{31} I_{s1} + A_{32} I_{s2} \\ \frac{d \hat{\varphi}_{s\beta}}{dt} &= -R_s i_{s\beta} + v_{s\beta} + A_{41} I_{s1} + A_{42} I_{s2} \end{aligned} \right. \quad (26)$$

where:

$A_i = \begin{bmatrix} A_{i1} & A_{i2} \\ A_{i3} & A_{i4} \end{bmatrix}$: Matrix of gains related to the stator current observation.

$A_\varphi = \begin{bmatrix} A_{\varphi1} & A_{\varphi2} \\ A_{\varphi3} & A_{\varphi4} \end{bmatrix}$: Matrix of gains related to the stator flux observation.

The sign vector is given by Eq.(27).

$$I_s = \begin{bmatrix} I_{s1} \\ I_{s2} \end{bmatrix} = \begin{bmatrix} \text{sign}(S_1) \\ \text{sign}(S_2) \end{bmatrix} \quad (27)$$

4.2.1 Determining the sliding surface

The sliding surface is a function of the current observation errors. Accordingly,

$$S = \begin{bmatrix} S_1 \\ S_2 \end{bmatrix} = \frac{1}{\sigma L_s (\frac{1}{T_r^2} + \omega^2)} \begin{bmatrix} \frac{1}{T_r} & -\omega \\ \omega & \frac{1}{T_r} \end{bmatrix} \begin{bmatrix} e_1 \\ e_2 \end{bmatrix} \quad (28)$$

where: $e_1 = i_{s\alpha} - \hat{i}_{s\alpha}$, $e_2 = i_{s\beta} - \hat{i}_{s\beta}$

$T_r = \frac{L_r}{R_r}$: Rotor time constant

The switching of the sliding surface S creates an oscillation phenomenon. To decrease the oscillation a saturation function can be introduced to replace the sign function. The saturation function is given in Fig. 9.

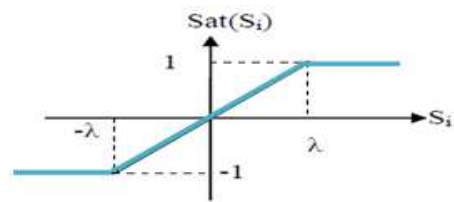


Fig. 9. Saturation function

$$\text{sign}(S_i) = \begin{cases} 1 & \text{si } S_i > \lambda \\ -1 & \text{si } S_i < -\lambda \\ \frac{S_i}{\lambda} & \text{si } |S_i| < \lambda \end{cases} ; i = 1, 2 \quad (29)$$

where λ is a positive constant with a low value.

4.2.2 Determining the gain matrices

The matrix of gains related to the current observer is as follows:

$$A_i = \begin{bmatrix} A_{i1} & A_{i2} \\ A_{i3} & A_{i4} \end{bmatrix} = \Gamma \begin{bmatrix} \delta_1 & 0 \\ 0 & \delta_2 \end{bmatrix} \quad (30)$$

where δ_1 and δ_2 are two positive constants, which are determined by applying the stability conditions defined by the Lyapunov approach.

The correction gains of the stator flux are determined by applying the condition of convergence towards the sliding surface ($S = 0$). The gain matrix of the stator flux is as follows:

$$A_\varphi = \begin{bmatrix} A_{\varphi1} & A_{\varphi2} \\ A_{\varphi3} & A_{\varphi4} \end{bmatrix} = \begin{bmatrix} q_1 \delta_1 & \frac{\omega}{\sigma L_s} \\ -\frac{\omega}{\sigma L_s} & q_2 \delta_2 \end{bmatrix} \quad (31)$$

where q_1 and q_2 are two positive constants.

4.2.3 Mechanism of adaptation of the stator resistance

The sliding mode observer is sensitive to the variations in the machine parameters. It is necessary to adjust the stator resistance of the machine by adding an adaptation mechanism. To determine the estimated stator resistance we have used the Lyapunov approach which is given by Eq.(32).

$$V = \frac{1}{2} S^T S + \frac{\lambda}{2} \left(\hat{R}_s - R_s \right)^2 \quad (32)$$

$$\dot{V} = S^T \dot{S} + \lambda \left(\hat{R}_s - R_s \right) \dot{\hat{R}}_s < 0 \quad (33)$$

To satisfy the condition defined by Eq.(33), the estimate of the stator resistance is given by Eq.(34):

$$\dot{\hat{R}}_s = -\gamma \int \left(\hat{i}_{s\alpha} * (i_{s\alpha} - \hat{i}_{s\alpha}) + \hat{i}_{s\beta} * (i_{s\beta} - \hat{i}_{s\beta}) \right) dt \quad (34)$$

with γ being a positive constant.

The structure of the predictive DTC-SVM with the adaptative SMO of an induction motor is shown in Fig. 10.

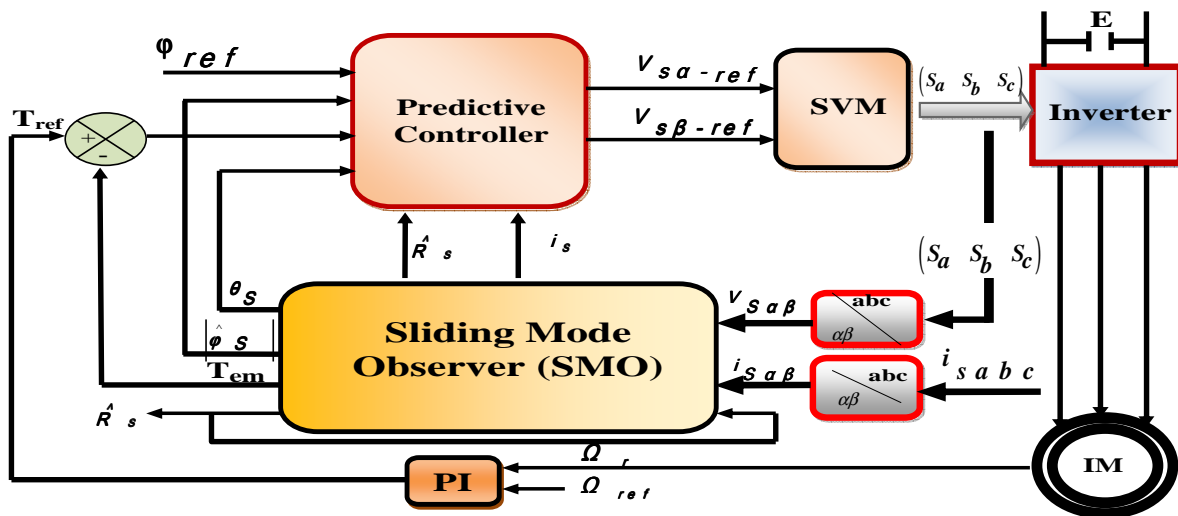


Fig. 10. Schematic of DTC-SVM with an SMO

5 Design of the SMO using the XSG

The components of the observed stator current vector for the system in equation (26) are illustrated using the XSG, as shown in Fig. 11.

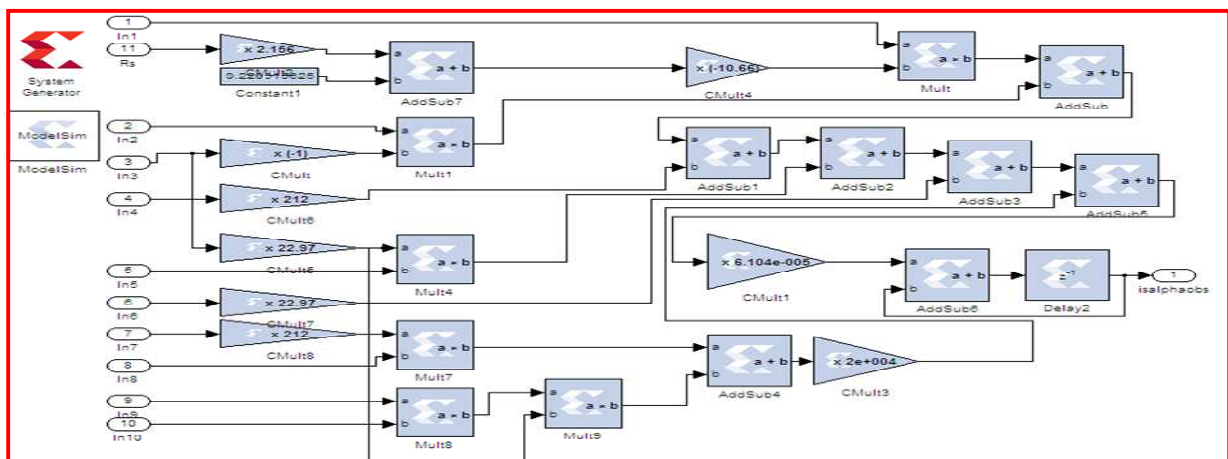


Fig. 11. Design of the Component $\hat{i}_{s\alpha}$ from the XSG

The sliding surface and saturation function, given in Eqs.(28) and (29) respectively, are

illustrated using the XSG, as shown in Fig. 12.

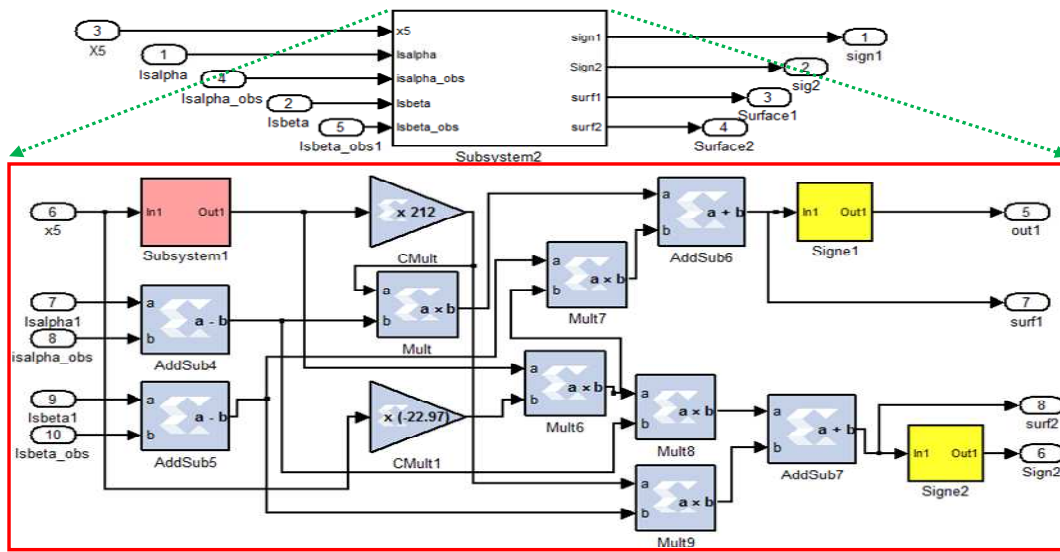


Fig. 12. Design of the sliding surface and sign function from the XSG

The gain matrix given in Eqs.(30) and (31),

respectively, are illustrated using the XSG, as shown in Fig. 13.

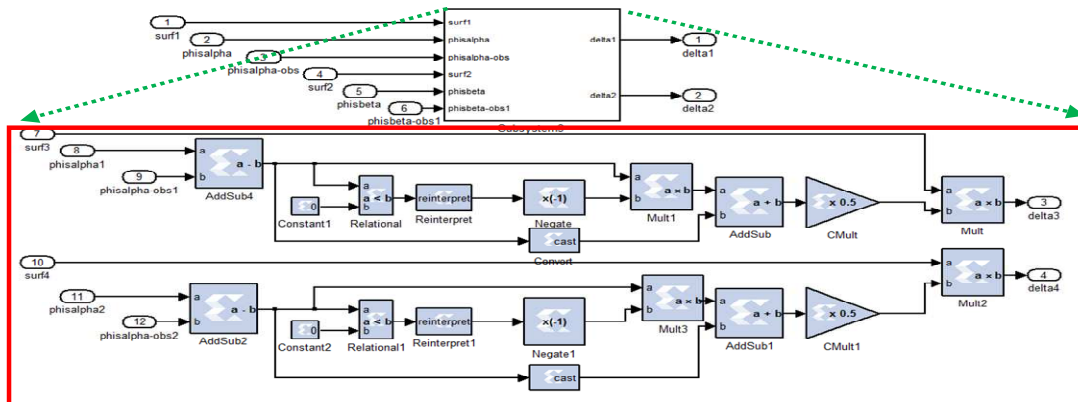


Fig. 13. Design of gains matrix

6 Simulation result

6.1 Testing the effectiveness and performance of the predictive DTC-SVM

The simulation of the conventional DTC and the predictive DTC-SVM is achieved using the XSG. The speed, torque and flux references, used in the simulation results of the direct torque control strategy, are $\Omega_{ref}=150\text{rad/s}$ and $\varphi_{ref} = 0.91(\omega b)$, respectively. At the time $t = 1\text{sec}$, a load torque of 10 Nm is applied. The induction motor parameters are in the Appendix.

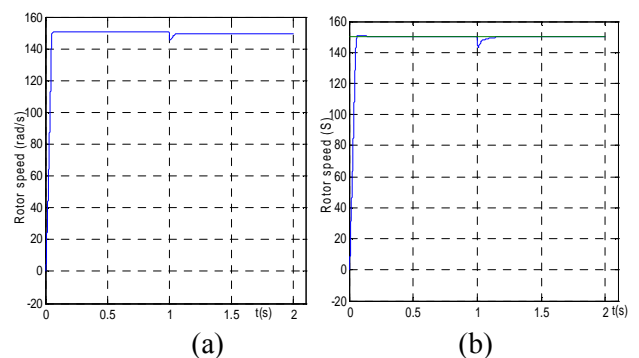


Fig. 14. Evolution rotor speed for: (a) Conventional DTC (b) Predictive DTC-SVM

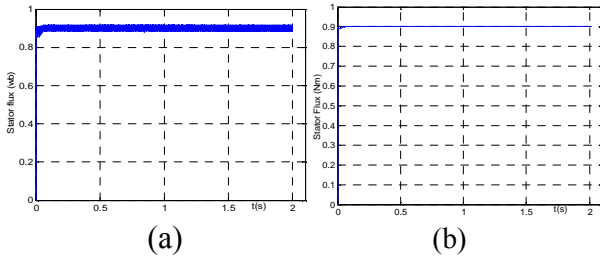


Fig. 15. Evolution of the real stator flux for: (a) Conventional DTC (b) Predictive DTC-SVM

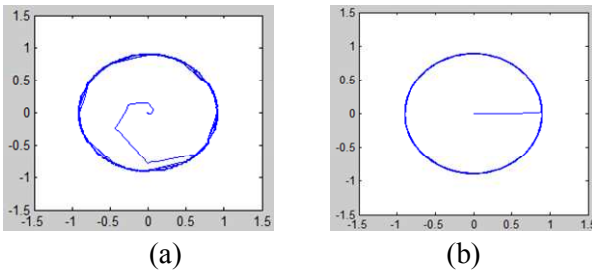


Fig. 16. Trajectory of the extremity of the stator flux vector for: (a) Conventional DTC, (b) Predictive DTC-SVM

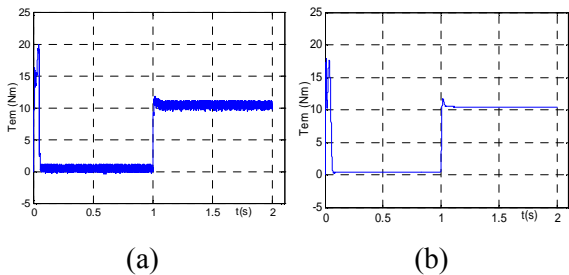


Fig. 17. Electromagnetic torque for: (a) Conventional DTC (b) Predictive DTC-SVM

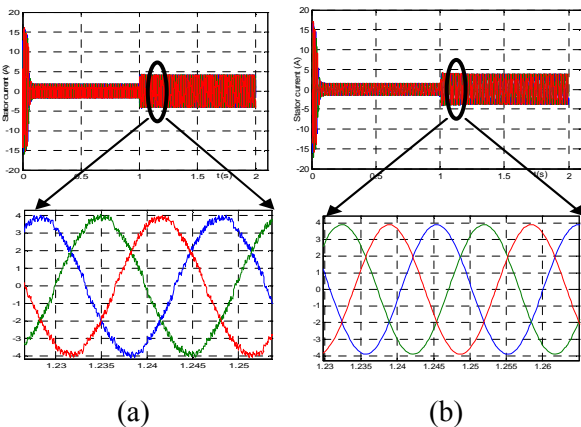


Fig. 18. Evolution of the stator current for: (a) Conventional DTC (b) Predictive DTC-SVM

6.2 Testing the effectiveness and performance of the predictive DTC-SVM with an SMO

The simulation of the predictive DTC-SVM with an open loop estimator and the predictive DTC-SVM

with an SMO is achieved using the XSG at a low speed. The speed and flux references used in the simulation results are 15 rad/s and 0.91 wb, respectively. At the time $t = 0.5\text{sec}$, a load torque of 5 Nm is applied. At $t = 1\text{sec}$, the stator resistance increases by 100%.

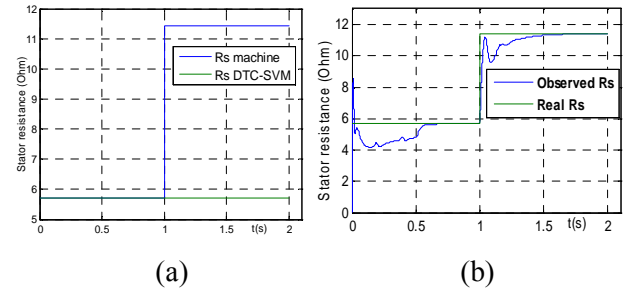


Fig. 19. Variation of R_s for Predictive DTC-SVM with: (a) an open loop estimator, (b) an SMO

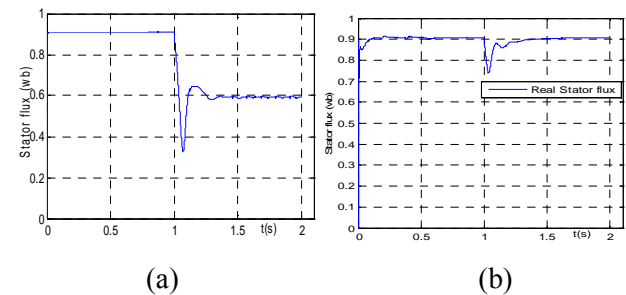


Fig. 20. Evolution of the stator flux for Predictive DTC-SVM with: (a) an open loop estimator, (b) an SMO

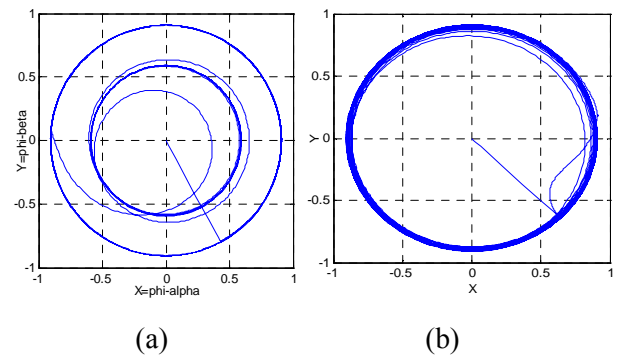


Fig. 21. Trajectory of the extremity of the stator flux vector for predictive DTC-SVM with: (a) an open loop estimator, (b) an SMO

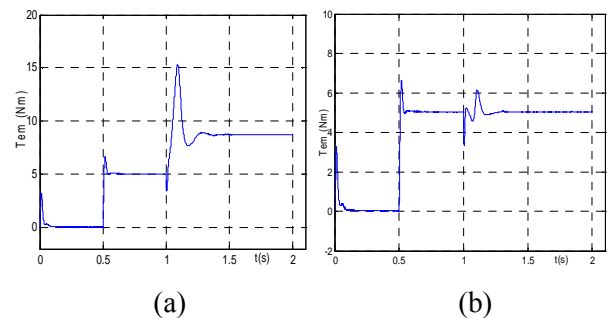


Fig. 22. Estimated electromagnetic torque for predictive DTC with: (a) an open loop estimator (b) an SMO

We obtain in Fig. 14, Fig. 15, Fig. 16, Fig. 17 and Fig. 18 the evolution of the mechanical speed, the stator flux magnitude, the stator flux vector trajectory, the electromagnetic torque and the stator current, respectively, for both conventional DTC and predictive DTC-SVM. These results show the effectiveness of the predictive DTC-SVM control relative to the conventional DTC control in terms of ripples in the stator flux and electromagnetic torque and in terms of distortion in the stator current.

In Fig. 19, the real stator resistance increases by 100%. In Fig. 19a, we can see that for the predictive DTC-SVM with the open loop estimator the stator resistance keeps constant; whereas, in Fig. 19b for the predictive DTC-SVM with an SMO, the observed stator resistance increases gradually to reach the resistance of the machine. Therefore, the SMO can compensate the variation of the stator resistance thanks to its good performance and robustness.

In Fig. 20a, at $t = 1\text{sec}$, the real stator flux decreases and the error between the real flux and the reference flux remains constant. Yet, in Fig. 20b, for the predictive DTC-SVM with an SMO, this error gradually vanishes.

In Fig. 21a, we can notice that the stator flux vector trajectory increases due to the variation of the stator resistance at $t=1\text{sec}$. By contrast, in Fig. 21b the stator flux trajectory remains constant thanks to the presence of the adaptive online mechanism of the stator resistance using the SMO.

In Fig. 22a, at $t = 1\text{sec}$, the electromagnetic torque increases and the error between the electromagnetic torque and the load torque remains constant. However, in Fig. 22b, for the SMO, this error vanishes quickly.

Fig. 23 illustrates the complete model of the DTC-SVM, which consists of an induction machine, an SMO, a torque controller, a proportional integral controller of speed, a calculator of the angle Θ , a predictive controller, an SVM block and a voltage source inverter.

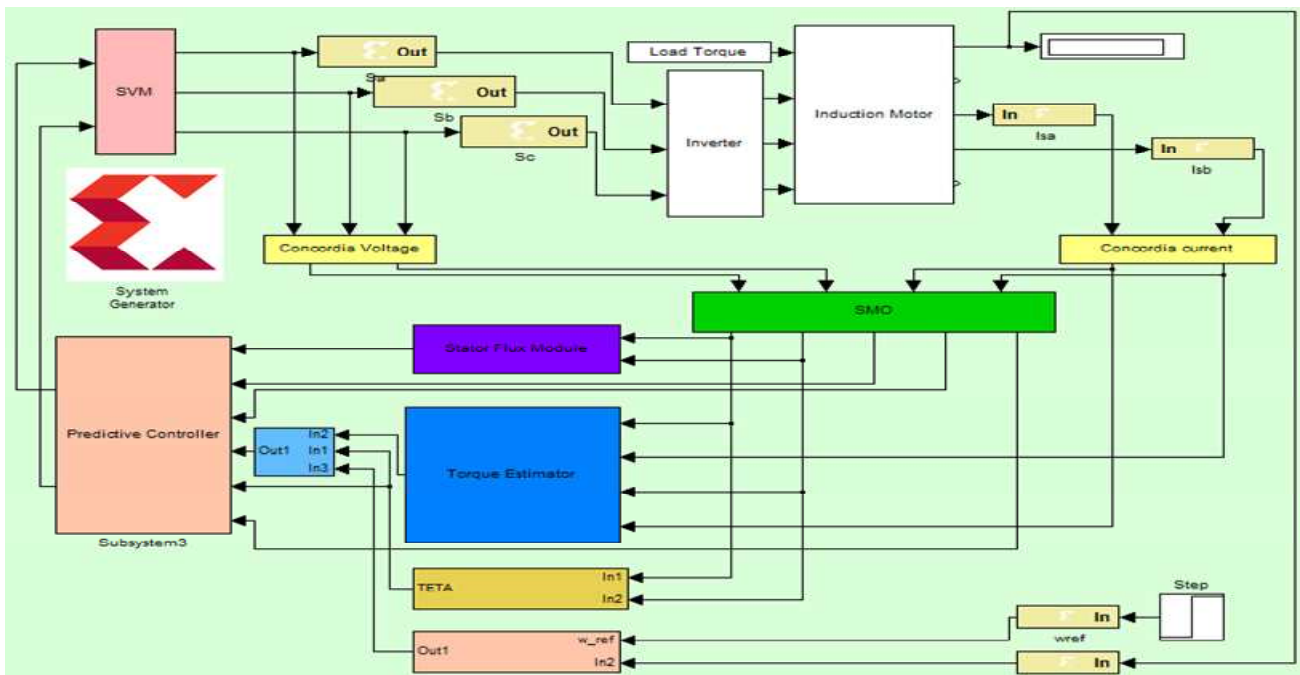


Fig. 23. Design of the predictive DTC-SVM with an SMO from the XSG

7 Implementation Results

The register transfer level (RTL) schematic of the predictive DTC-SVM with an SMO in the Xilinx

Integrated Synthesis Environment (ISE) 12.4 is given in Fig. 24.

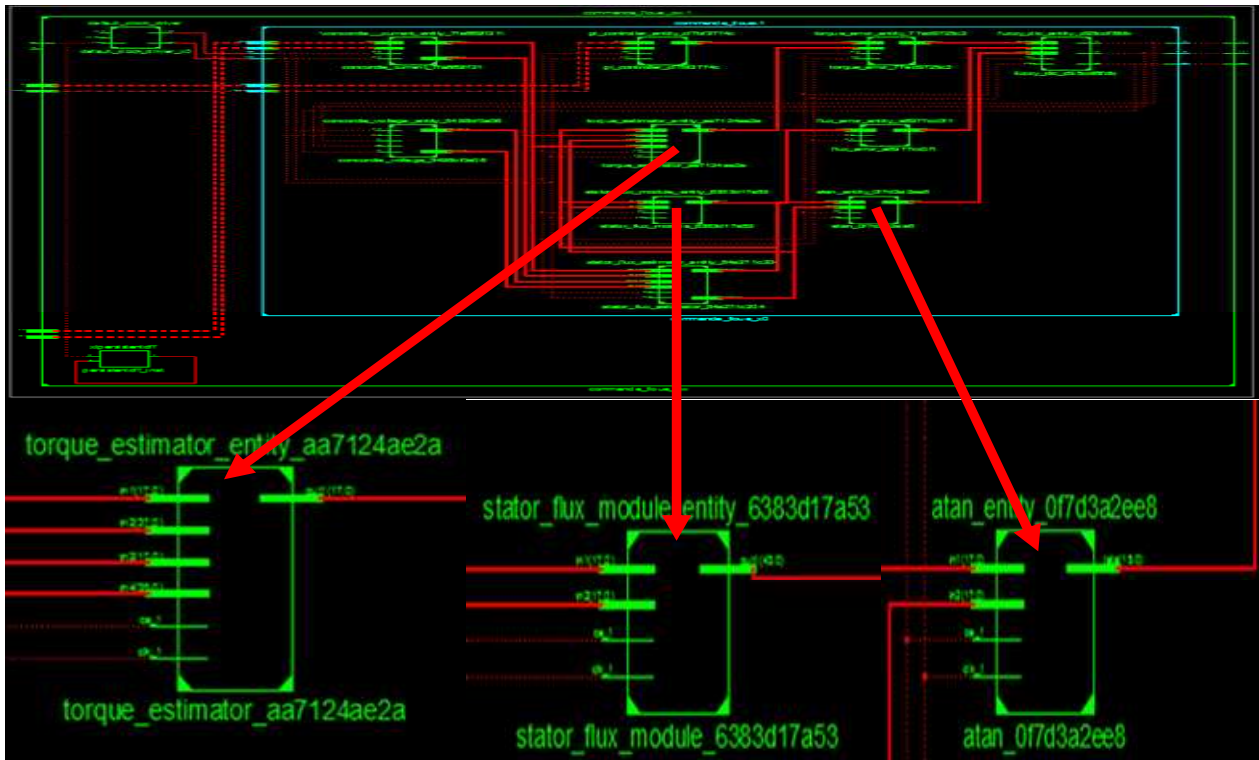


Fig. 24. The schematic RTL of the predictive DTC SVM

Table 2. Used resources

	Used	
	DTC	Predictive DTC
Number of bonded IOBs	68	68
Number of Slices	259	473
Number of Slice LUTs	1344	1601
Number of DSP48Es	12	14

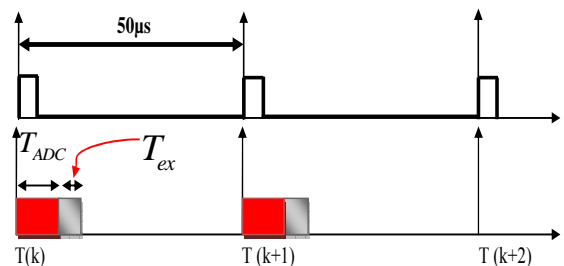


Fig. 25. Timing diagram for the implementation of the predictive DTC-SVM with an SMO using Xilinx Virtex-V FPGA with an xc5vfx70t-3ff1136 package

The performance of the hardware solution based on the FPGA in terms of execution time is shown in Fig. 25. Table 3 presents the performance time of the predictive DTC-SVM with an SMO.

t_{ADC} : Analogue to digital conversion time.

Table 3. Execution time T_{ex}

Module	Execution time (μs)
Concordia	0.17
Sliding Mode Observer (SMO)	0.34
Predictive controller	0.12
SVM	0.14
PI controller	0.16
$t_{predictive_DTC-SMO} = 0.17 + 0.34 + 0.12 + 0.14 + 0.16 = 0.93 \mu s$	0.93 μs
Total Time: $T_{total} = t_{predictive_DTC-SMO} + t_{ADC}$	

Papers [22],[23] and [24] present the digital control of induction motor using the dSPACE 1104, in these papers the sampling time is to 100 μs , due to the sequential processing of the dSPACE. In paper [25], the execution time is of 300 μs using dSPACE 1102. Using the FPGA the execution time of the control algorithm of induction motor is (1 to 2 μs). Therefore, the obtained execution time using the FPGA is far lower compared to the software solutions. In this paper the execution time of the predictive DTC-SVM with the SMO algorithm is of 0.93 μs using the Xilinx Virtex-V FPGA with an xc5vfx70t-3ff1136 package.

8 Conclusion

In this paper, the direct torque control of an induction motor based on the Space vector modulation, the predictive controller and the sliding mode observer has been developed. The hardware architectures of the predictive DTC-SVM and the sliding mode observer using the Xilinx system generator are presented. The simulation results show the performances of the proposed control strategy in terms of ripples of the electromagnetic torque and the stator flux, distortion of the stator current, and variation of the machine parameters. The VHDL code is generated and synthesized. The implementation results show the performances of the hardware implementation in terms of design time which is reduced, minimal resources utilization, and low execution time.

APPENDIX

Table 4. Motor parameters

Parameter	Value
R_s	5.717 Ω
R_r	4.282 Ω
L_s	464 mH
L_r	464 mH
M	441.7 mH
J	0.0049 Kg.m ²
P	1.5 kW
V/U	230/400 V

References:

- [1] A. V. Deshmukh, *Microcontrollers, Theory and Applications*, ser. The Companies, Computer Engineering Series. New York: Mac-Graw-Hill, 2007.
- [2] P. Lapsley, *DSP Processor Fundamentals: Architecture and Features*. Piscataway, NJ: IEEE Press, 1997.
- [3] W. H. Wolf, *FPGA-Based System Design*. Englewood Cliffs, NJ: Prentice-Hall, 2004.
- [4] B. K. Bose, "Modern power electronics and AC drives", Condra Chair of Excellence in Power Electronics, the University of Tennessee, Knoxville.2002.
- [5] M.Dепенbrock, "Direct self-control (DSC) of inverter fed induction machine", IEEE Transactions on Power Electronics, Vol 3, N°4, 420-429, 1988.
- [6] T. Noguchi, and I.Takahashi, "Quick torque response control of an induction motor based on a new concept", (in Japanese), IEEJ Tech. Meeting Rotating Mach., RM 84-76, 61-70, 1984.
- [7] I. Takahashi, and T. Noguchi, "A new quick-response and high efficiency Control strategy of an induction machine", IEEE Transactions Industry Applications, Vol. 22,N°5, 820- 827, 1986.
- [8] G. S. Buja and M. P. Kazmierkowski, "Direct torque control of PWM inverter-fed AC motors-A survey", IEEE Transactions Industry Electronics., vol. 51, N° 4, pp. 744757, 2004.
- [9] I. Takahashi, Y.Ohmori, "High-performance Direct Torque Control of an Induction Motor ", IEEE Transactions on Industry Applications, Vol. 25, N°2, pp. 257-264, 1989.
- [10] R. Ramya, C. Abhijith, S. Raju, "DTC AND IFOC: feasibility analysis on torque control schemes of an induction motor", Undergraduate Academic Research Journal (UARJ), Vol.2, N° 3, 4, 2012.
- [11] D.Casadei, G. Serra, K. Tani, "Implementation of a direct control algorithm for induction motors based on discrete space vector modulation", IEEE Transactions Power Electronics, , vol. 15, N° 4, pp. 769-777, 2000.
- [12] Y. S. Lai, J. H. Chen, "A new approach to direct torque control of induction motor drives for constant inverter switching frequency and torque ripple reduction", IEEE Transactions Energy Conv. vol. 16, N°3, pp. 220-227, 2001.
- [13] M. Barut, S. Bogosyan, M.Gokasan, "Speed sensorless direct torque control of IMs with rotor resistance estimation", International Journal Energy Conv. and Manag, 46, N°3, pp. 335-349, 2005.
- [14] D. Casadei, F. Profumo, G. Serra, A. Tani, "FOC and DTC: Two Viable Schemes for Induction Motors Torque Control", IEEE Transaction on Power Electronics, Vol. 17, N° 5, pp. 779 - 787, Sept. 2002.
- [15] S. Meziane, R. Toufouti and H. Benalla, "Speed Sensorless Direct Torque Control and Stator Resistance Estimator of Induction Motor Based MRAS Method", International Journal of Applied Engineering Research (IJAER), Vol. 3, N° 6, pp. 733-747, 2008.
- [16] M. Messaoudi, H. Kraiem, M. Ben Hamed, L. Sbitta, and M. N. Abdelkrim, A Robust Sensorless Direct Torque Control of Induction Motor Based on MRAS and Extended Kalman

- Filter," Leonardo Journal of Sciences, Academic Direct issue 12.
- [17] Xilinx System Generator v2.1 for Simulink User's Guide Online.
www.mathworks.com/applications/dsp_comm/xilinx_ref_guide.pdf;
- [18] J.G. Mailloux; Prototypage Rapide de la Commande Vectorielle sur FPGA à l'Aide des Outils SIMULINK-SYSTEM GENERATOR, l'Université de Québec, Mars 2008 ;
- [19] White paper: Using System Generator for Systematic HDL Design, Verification, and Validation WP283 (v1.0) January 17, 2008.
- [20] A. MAHFOUZ, W.M. MAMDOUH, "Intelligent DTC for PWSM Drive using ANFIS technique", International Journal of Engineering Science and Technology(IJEST), Vol. 4,N°. 03, pp 1208-1222, March 2012.
- [21] Murai, Gohshi Y, Matsui K, Hosono I, High frequency split zero-vector PWM with harmonic reduction for induction motor drive. IEEE Trans Ind Appl 28(1):105–112,1992.
- [22] Bhoopendra Singh, Shailendra Jain, and Sanjeet Dwivedi, "Direct Torque Control Induction Motor Drive with Improved Flux Response". Hindawi Publishing Corporation Advances in Power Electronics, Article ID 764038, pp.1-11. Vol.2012.
- [23] ELBACHA, Z. BOULGHASOUL and E. ELWARRAKI, A Comparative Study of Rotor Time Constant Online Identification of an Induction Motor Using High Gain Observer and Fuzzy Compensator", WSEAS TRANSACTIONS on SYSTEMS and CONTROL, Vol 7, N°2, pp.37-53, 2012.
- [24] Vojkan Kostić, Milutin Petronijević, Nebojša Mitrović, Bojan Banković, "Experimental verification of direct torque control methods for electric drive application", Automatic Control and Robotics Vol. 8, No 1, pp. 111 – 126, 2009.
- [25] M. Boussak and K. Jarray, "A High-Performance Sensorless Indirect Stator Flux Orientation Control of Induction Motor Drive". IEEE Transactions on industrial electronics, Vol. 53, No. 1, pp.14-49, 2006.